Research Article

Developing a new method for synthesizing amine functionalized g-C_3N_4 nanosheets for application as anti-corrosion nanofiller in epoxy coatings

Sepideh Pourhashem[1] · Alimorad Rashidi[1] · Mahshad Alaei[1] · Mohammad-Amin Moradi[2] · Davood Mohammady Maklavany[1]

Abstract

In this research, the effect of graphitic carbon nitride (g-C_3N_4) on the corrosion protection performance of solvent-based epoxy coatings is investigated. The g-C_3N_4 is synthesized by two-step condensation of melamine and is characterized by X-ray diffraction, Fourier transform infrared spectroscopy, transmission electron microscopy, and carbon–hydrogen–nitrogen elemental analysis. In order to enhance the dispersion of g-C_3N_4 in epoxy coating, it is chemically functionalized with ethylenediamine vapor via a simple method. Further, epoxy coatings containing different amounts (0, 0.05, 0.1, 0.3, 0.5, and 0.7 wt%) of amine functionalized g-C_3N_4 (AF g-C_3N_4) are spray coated on mild steel substrate. The dispersion quality of nanofillers in coating matrix is studied by field emission scanning electron microscopy. The corrosion resistance of samples is investigated by electrochemical impedance spectroscopy. The results reveal the superior corrosion protection of nanocomposite coatings due to barrier performance of AF g-C_3N_4. Meanwhile, epoxy coating containing 0.5 wt% AF g-C_3N_4 shows the highest corrosion protection compared to pure epoxy sample.

Keywords g-C_3N_4 · Amine functionalization · Nanocomposite epoxy coating · Corrosion

1 Introduction

Metallic structures thermodynamically tend to decrease their energy and corrode in the presence of corroding agents including water and oxygen [1]. Corrosion phenomenon causes notable economic loss and it is a serious threat for industries [2]. In this regard, organic coatings can provide corrosion protection for metallic materials [3]. Among polymer protective coatings, epoxy coatings are extensively used due to their high adhesion onto various substrates, high chemical resistance, and versatility [4, 5]. However, epoxy coatings have some drawbacks such as high brittleness, notch sensitivity, developing micro-pores during solvent evaporation, hydrolytic degradation, and low barrier performance [6, 7].

In recent years, graphene derivatives have been widely employed as nanofiller to boost the corrosion resistance of epoxy coatings. Polymer coatings containing graphene based nanomaterials possess outstanding properties which can be assigned to inherent nature of graphene derivatives regarded as high surface area, low density, high aspect ratio, excellent mechanical strength, and advanced barrier effect against gases and corrosive agents [8–10]. Graphene [8, 9, 11, 12], functionalized graphene [13, 14], graphene oxide [15–17], graphene oxide nanosheets functionalized with various agents including silane [18], amine [19], and urea–formaldehyde [4], graphene oxide

✉ Alimorad Rashidi, rashidiam@ripi.ir | [1]Nanotechnology Research Center, Research Institute of Petroleum Industry (RIPI), West Entrance Blvd., Olympic Village, P.O. Box 14857-33111, Tehran, Iran. [2]Laboratory of Materials and Interface Chemistry and Centre for Multiscale Electron Microscopy, Department of Chemical Engineering and Chemistry, Eindhoven University of Technology, 5600 MB Eindhoven, The Netherlands.

SN Applied Sciences (2019) 1:108 | https://doi.org/10.1007/s42452-018-0123-7

Received: 29 September 2018 / Accepted: 12 December 2018 / Published online: 17 December 2018

modified with nanoparticles such as silica [20], titania [21], and alumina [22] are regarded as different types of graphene based nanomaterials developed for providing highly corrosion resistant coatings.

Moreover, graphitic carbon nitride (g-C_3N_4) is a two dimensional nanomaterial with similar layered structure of graphene; indeed, strong C–N covalent bonding presents in the plane direction and the planes are packed together through van der Waals interactions. In recent years, g-C_3N_4 has attracted a great attention because of relative ease of synthesis, non-toxicity, and high chemical, physical, and thermal stability [23–26]. Compared to graphene based nanofillers, g-C_3N_4 possesses unique advantages as simple preparation procedure, low cost, and semiconductor behavior [3, 27]. In addition, the g-C_3N_4 with sheet-like morphology and high aspect ratio can increase the tortuosity of diffusion path of corrosive agents in polymer matrix and therefore, improve the corrosion protection efficiency of polymer based coatings. Accordingly, Zuo et al. [3] proved that polyaniline modified g-C_3N_4 is appropriate nanofiller for enhancing the corrosion resistance of epoxy coatings.

It should be mentioned that during our previous studies, we have prepared nanocomposite epoxy coatings containing graphene oxide [15], silane functionalized graphene oxide [7, 18], and silica decorated graphene oxide [20]; revealing that nanofillers with sheet-like morphology are appropriate candidate for developing highly corrosion resistant coatings. Our previous studies showed that the wt% of nanofiller in polymer matrice as well as the functional groups on the surface of nanofillers are key parameters for achieving nanocomposites with high corrosion resistance. In this research, melamine, which has honey-comb atomic arrangement close to g-C_3N_4, is used as a very cheap and abundant nitrogen containing precursor for synthesizing g-C_3N_4 [28]. The g-C_3N_4 is synthesized via melamine pyrolysis. This is a simple and economic approach for synthesizing corrosion resistant nanofiller with high surface-to-volume ratio and sheet-like morphology. However, g-C_3N_4 nanosheets poorly disperse in polymer matrix [29] due to the presence of strong van der Waals interactions and π–π stacking [30, 31]. Since, the distribution of nano-additives plays an important role in enhancing the properties of polymer composite, the dominant challenge of g-C_3N_4 application in epoxy coating is to develop methods for improving the dispersion quality of g-C_3N_4 in polymer matrix.

Here, we have employed the strategy of directly adding the amine functionalized g-C_3N_4 nanosheets to hardener in order to improve the distribution of g-C_3N_4 in epoxy coating. The developed strategy has three main reasons: First of all, it has been demonstrated that nanosheets have high tendency to disperse in lower-viscosity medium [15, 32, 33]. Accordingly, due to lower viscosity of hardener compared to epoxy resin, the dispersion of nanosheets in hardener is better than epoxy resin; therefore, the g-C_3N_4 nanosheets are directly added to hardener. Second, since the hardener used in this research has amine groups, the prepared g-C_3N_4 is chemically modified with amine in order to enhance the compatibility between nanofiller and the hardener. Third, the vapor of ethylenediamine is used for functionalizing the g-C_3N_4 nanosheets. This procedure involves reacting carboxylic acid moieties developed on g-C_3N_4 nanosheets via HNO_3 vapor with vapors of ethylenediamine. The advantages of this procedure can be regarded as: g-C_3N_4 remains in a dry state; there is no need for separation, filtration, washing, and drying steps; the morphology and agglomeration degree of g-C_3N_4 nanosheets will not deteriorate [34, 35]. Further, the effect of amine functionalized g-C_3N_4 nanosheets on corrosion protection performance of solvent-based epoxy coating is investigated.

2 Experimental

2.1 Materials

All chemicals were analytical grade reagents without further purification. Melamine ($C_3H_6N_6$) was purchased from Uroumiyeh Petrochemical Co. Iran. Ammonium carbonate ($(NH_4)_2CO_3$), nitric acid (HNO_3) and ethylenediamine ($C_2H_4(NH_2)_2$) were obtained from Sigma-Aldrich. For preparing epoxy coatings, Bisphenol F type epoxy resin and its polyamide hardener with the weight mixing ratio of 10: 1 (resin to hardener) were purchased from Kian Co. Iran. Mild carbon steel plates (ST-12, Foolad Mobarakeh Co., Iran) are used as metallic substrate. These panels were sandblasted, cleaned with acetone and blow-dried before applying coatings on them.

2.2 Synthesis of g-C_3N_4

The g-C_3N_4 is synthesized by three step condensation of melamine. 14 g melamine is added to 280 mL deionized water while stirring for 30 min. Then, it is transferred into 420 mL Teflon-lined autoclave and heat treated at 200 °C for 24 h. The precipitate is filtered and dried at 80 °C to obtain a white powder. The derived white powder is mixed and ground in agate mortar with equal amount of ammonium carbonate. Then, the mixture is added into DI water and stirred at 80 °C until dried completely. The dry mixture is put into alumina crucible with a cover and heated at 600 °C for 4 h in a muffle furnace with heating rate of 5 °C/min. The synthesized yellow powder is denoted as nano g-C_3N_4.

In the first step, melamine is condensed hydrothermally and ammonia is generated through condensation of melamine. Then, in the second step, as-condensed melamine gradually polymerized with increasing the temperature in the presence of ammonium carbonate; ammonium carbonate ($(NH_4)_2CO_3$) decomposes into NH_3, CO_2, and H_2O gases which act as dynamic gas template, preventing the aggregation of melamine and producing two-dimensional g-C_3N_4 [25].

2.3 Synthesis of amine functionalized g-C_3N_4

In the first step, the g-C_3N_4 is oxidized with HNO_3 vapor. In this procedure, the synthesized g-C_3N_4 is loaded in the reactor heated at 125 °C. The concentrated HNO_3 is loaded in the round bottom flask which is heated and stirred at 125 °C. After 24 h, the oil bath heating is turned off and the heater of reactor is turned off after 1 h in order to dry the functionalized g-C_3N_4. Then, the oxidized g-C_3N_4 is collected from the reactor. In the second step, ethylenediamine is used for amine functionalization of oxidized g-C_3N_4. The oxidized g-C_3N_4 is placed in the reactor heated at 165 °C. The bottom flask is loaded with ethylenediamine which is heated and stirred at 165 °C. The reaction is maintained for 8 h and then, the oil bath heating is turned off. After 1 h, the heater of reactor is turned off in order to obtain dry amine functionalized g-C_3N_4. The amine functionalized g-C_3N_4 is abbreviated as AF g-C_3N_4. In the proposed procedure, the g-C_3N_4 is only treated with vapor and it is not in contact with liquid, leading to achieve functionalized g-C_3N_4 without losing the material. The HNO_3 and ethylenediamine vapors can continuously pass through the column; indeed, the vapors can circulate via refluxing in the two neck flask and return into round bottom flask by condensing in the attached condenser.

2.4 Preparation of nanocomposite coatings

To prepare epoxy composite coatings containing 0, 0.05, 0.1, 0.3, 0.5, and 0.7 wt% AF g-C_3N_4, the required amount of AF g-C_3N_4 is directly added to hardener and sonicated for 5 min. Then, the mixture is added to stoichiometric amount of epoxy resin and mechanically mixed to obtain a uniform dispersion. In the next step, they are diluted with thinner and spray coated on mild steel panels. Finally, the samples are kept for 24 h at room temperature and then, heated at 90 °C for 2 h to complete curing reactions.

2.5 Characterizations

The crystal structure of g-C_3N_4 is characterized by X-ray diffraction analysis (XRD, Philips PW 3710, 30 kV, 35 mA, Cu Kα). Carbon–Hydrogen–Nitrogen (CHN) elemental analysis is performed on the synthesized sample by using CHN elemental analyzer (FlashEN 1112, Thermo Finnigan). The morphology of g-C_3N_4 is observed by transmission electron microscopy (TEM, Philips, EM208S, 100 kV). The sample for TEM analysis is prepared by dispersing a small amount of g-C_3N_4 powder in ethanol by help of ultrasonic bath and then, dropping one drop of the prepared dispersion on grid and drying at room temperature before TEM test. Further, functionalization of g-C_3N_4 with HNO_3 and ethylenediamine is studied by Fourier transform infrared spectroscopy (FTIR, Vector 33 Bruker spectrometer) over wavelength range of 400–4000 cm^{-1}. The dispersion quality of amine functionalized g-C_3N_4 in coating matrix is considered by field emission scanning electron microscopy (FE-SEM, MIRA3 TESCAN).

2.6 Corrosion test

The electrochemical performance of samples is examined by electrochemical impedance spectroscopy (EIS) utilizing an Ivium electrochemical analyzer instrument (Compact Stat Ivium Software 2.775, Netherlands). Electrochemical behavior is measured by a three electrode cell consisting of coated substrate, platinum rod and saturated calomel electrode (SCE) as working, counter, and reference electrode, respectively. The NaCl solution with 3.5 wt% concentration is used as corrosive electrolyte. The EIS tests are carried out at OCP in frequency range of 10^{-2} to 10^5 Hz with AC amplitude of 10 mV after immersion in corrosive electrolyte for different times. The measurements are repeated 3 times to be ensure about the repeatability of data. The impedance spectra are analyzed by fitting the experimental data with the help of electrical equivalent circuit (EEC).

3 Results and discussion

3.1 Characterization of g-C_3N_4 nanosheets

The phase structure of g-C_3N_4 is examined by XRD (Fig. 1). The XRD pattern shows two distinct diffraction peaks at 12.8° and 27.8° which match with (100) and (002) crystal planes of g-C_3N_4, respectively. The low-intensity peak at $2\theta = 12.8°$ with d-spacing of 0.68 nm is due to in-plane structural repeating motifs of the continuous heptazine network. The main peak observed at $2\theta = 27.8°$ with d-spacing of 0.32 nm is attributed to the characteristic interlayer stacking peak of graphitic-like aromatic structure [26, 36, 37]. The XRD pattern presents that the graphitic carbon nitride is synthesized.

Table 1 shows the results of elemental analysis. Accordingly, the C/N atomic ration for g-C_3N_4 sample is 0.659

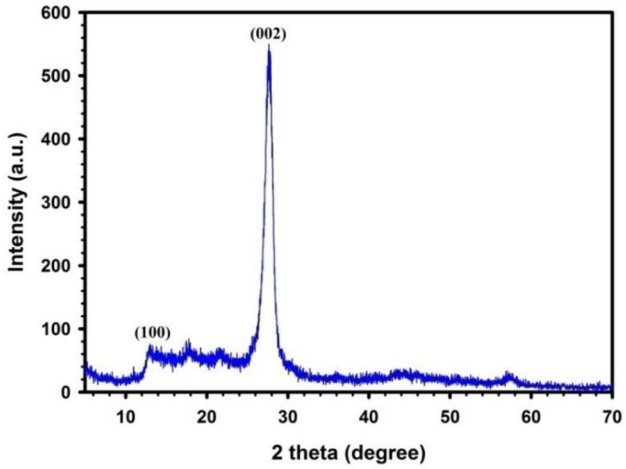

Fig. 1 XRD Pattern of g-C_3N_4

Table 1 Elemental analysis of the synthesized g-C_3N_4

Sample	Elemental analysis				
	C (wt%)	H (wt%)	N (wt%)	Others (wt%)	C/N (atomic)
g-C_3N_4	34.92	1.66	61.82	1.60	0.659

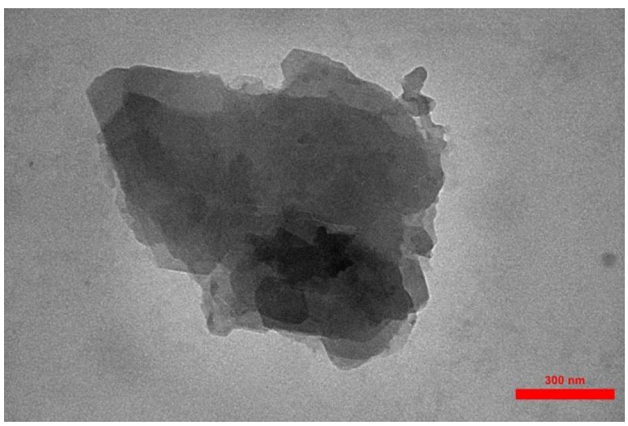

Fig. 2 TEM image of g-C_3N_4

which is lower than the theoretical value (0.75). The detection of H element in this sample can be attributed to formation of amine groups (C–NH_2 and C–NH) in g-C_3N_4 sample during synthesis procedure [38].

Figure 2 shows the TEM image of g-C_3N_4 which clearly indicates the layered plate-like morphology of g-C_3N_4 due to the graphitic structure of the sample. Further, TEM image shows the stacked layer structure.

The molecular structure of g-C_3N_4 before and after functionalization with HNO_3 and ethylenediamine is characterized by FT-IR. Figure 3 shows the FT-IR spectra of samples, proving their C-N skeleton. The broad peaks located at

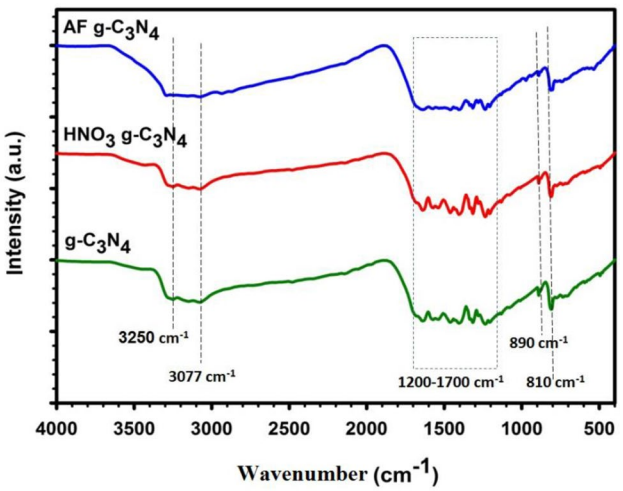

Fig. 3 FTIR spectra of g-C_3N_4, HNO_3 vapor treated g-C_3N_4, and amine functionalized g-C_3N_4

3250 and 3078 cm^{-1} are assigned to O–H and N–H bands, related to residual N–H groups and adsorbed H_2O molecules [38]. The absorption peaks at 1200–1600 cm^{-1} are assigned to stretching vibration of CN heterocyclic [39]. The peak at 890 cm^{-1} is related to deformation mode of N–H components [39]. The peak at 802 cm^{-1} is due to vibration of s-triazine units, indicating complete skeleton g-structure of g-C_3N_4 for all three samples [25]. In the case of HNO_3 treated sample, extra absorption peaks at 1540, 1280, 1132, and 735 cm^{-1} have appeared, attributed to N–H/C–N, C–O, C–O, and C–H vibrations, respectively. For AF g-C_3N_4, after functionalization with amine, the intensity of absorption peak at 3078 cm^{-1} enhances due to increase of amino groups on the surface of g-C_3N_4 sample.

3.2 Morphology of epoxy/AF g-C_3N_4 nanocomposites

Figure 4 shows the FE-SEM images from cross-section of pure epoxy and nanocomposite epoxy coatings containing different loadings of AF g-C_3N_4. The cross section image of pure epoxy coating (Fig. 4a) is smooth because it has brittle fracture behavior. Pure epoxy coating has brittle fracture and it contains no nanofiller; therefore, its fracture surface is smooth. Indeed, the cracks developed in the pure epoxy coating propagate freely in the matrix. However, the fracture surfaces of nanocomposite coatings are rough; indicating more ductile fracture mechanism due to presence of nanofillers which can prevent the crack propagation in polymer matrix [40]. In fact, by incorporating nanofillers in polymer matrice, the fracture mechanism changes from brittle to ductile. Further, the inhomogeneities seen in nanocomposite fracture surface are because of nanofillers dispersion in coating matrix which prevents the

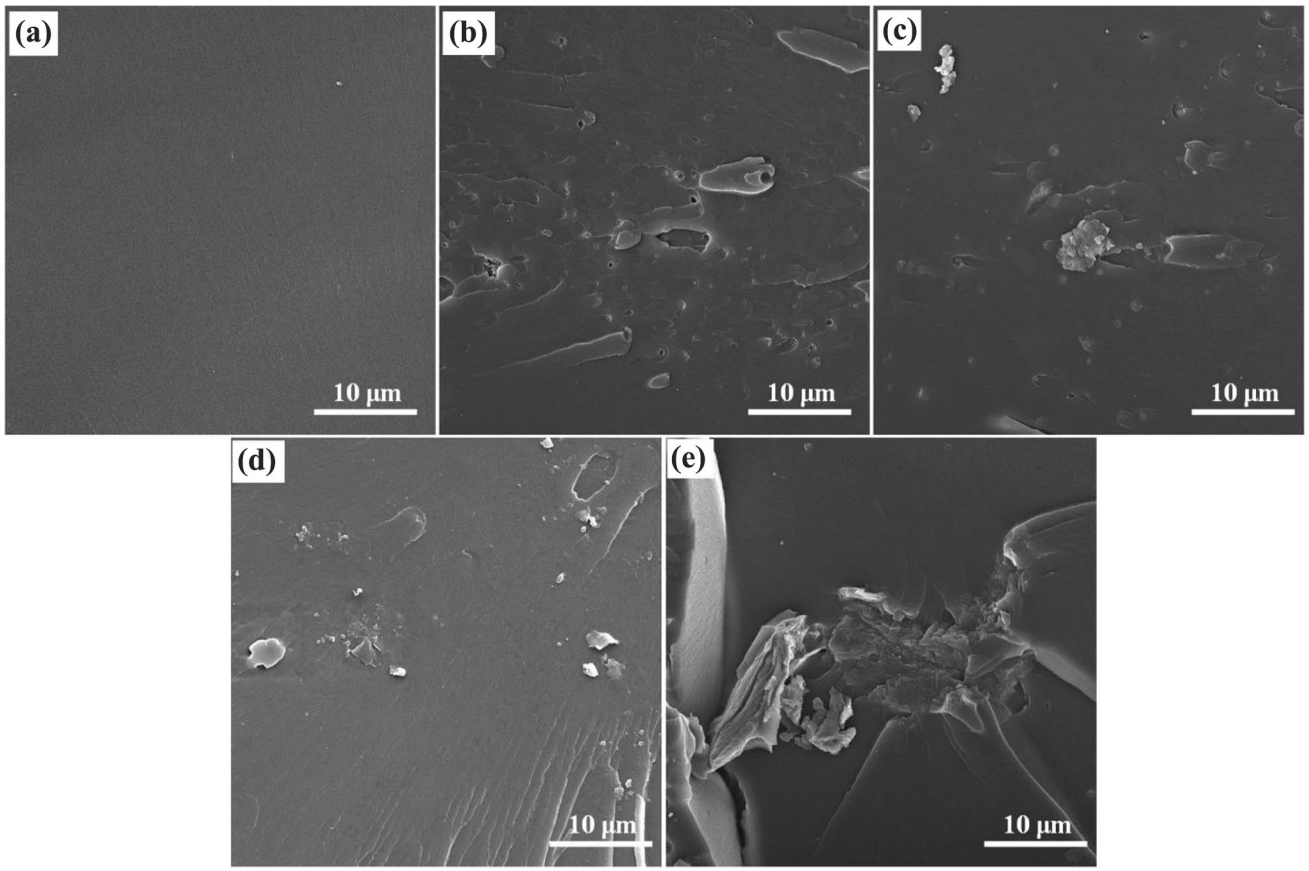

Fig. 4 FE-SEM images from cross section of **a** pure epoxy, **b** epoxy/0.1 wt% AF g-C_3N_4, **c** epoxy/0.3 wt% AF g-C_3N_4, **d** epoxy/0.5 wt% AF g-C_3N_4, and **e** epoxy/0.7 wt% AF g-C_3N_4

propagation of cracks. The dispersion quality of nanofillers within epoxy matrix is an important issue to achieve highly corrosion resistant coatings. As Fig. 4b presents, the fracture surface of epoxy coating containing 0.1 AF g-C_3N_4 is not uniform and some defects can be seen in the coating matrix; it can be attributed to insufficient amount of nanofiller in polymer matrix. According to Fig. 4b and c, when the amount of nanofiller is 0.1 and 0.3 wt%, the nanofillers could not disperse homogeneously inside polymer matrix. In the case of nanocomposite coating loaded with 0.5 wt% nanofiller (Fig. 4d), the nanofiller dispersion is more uniform compared to Fig. 4b, c and e. By increasing the loading of AF g-C_3N_4 to 0.3 and 0.5 wt%, the fracture surface becomes more uniform and in the case of epoxy/0.5 wt% AF g-C_3N_4, homogeneous dispersion of AF g-C_3N_4 in coating matrix with no defects in polymer matrix are observed, indicating good interface adhesion between nanofiller and matrix. As Fig. 4e presents, the agglomeration of nanosheets happens by increasing the wt% of AF g-C_3N_4 to 0.7% and the interfacial bonding between polymer and nanofiller becomes weak. Higher amounts of nanofiller (i.e. 0.7 wt%) leads to nonuniform dispersion of nanofiller in coating matrix and their agglomeration as well as cracks are clearly observed. Similar observations are previously reported by researches worked on polymer/graphene nanocomposite coatings [22, 40–43].

3.3 Corrosion protection performance of epoxy/AF g-C_3N_4 nanocomposite coatings

The corrosion protection performance of coatings is evaluated by EIS to study the effect of g-C_3N_4 on barrier behavior of epoxy coating. The Bode plots show the Impedance Modulus as a function of frequency which is very applicable for understanding the overall resistance of coating system against corrosive media. The Bode plots, exhibit high frequency region due to the coating capacitance and low frequency region due to charge transfer processes occurring at solution/coating interface. Since presenting electrochemical impedance spectroscopy results by Nyquist and Bode plots are a common way for exploring the corrosion resistance of coating systems [44–47], these plots are presented and discussed in this research.

Figures 5, 6 and 7 show the Bode and Nyquist diagrams of mild steel substrate coated with pure epoxy and epoxy/AF g-C_3N_4 coatings after immersion in 3.5 wt% NaCl solution for 2 h, 24 h, and 48 h, respectively. According to Bode plots, nanocomposite coatings show higher impedance modulus (|Z|) at low frequencies (10^{-2} HZ), indicating higher corrosion inhibition of composite samples compared to pure epoxy. The |Z| value depends on the amount of AF g-C_3N_4 loading in polymer matrice. The |Z| value increases by increasing the wt% of AF g-C_3N_4 in composite coating, revealing the enhanced barrier performance of AF g-C_3N_4 nanosheets. Epoxy/0.5 wt% AF g-C_3N_4 nanocomposite coatings show the highest |Z| value and by adding extra amounts of AF g-C_3N_4 nanosheets, the |Z| value decreases. Moreover, the |Z| value decreases by increasing immersion time, due to diffusion of corrosive agents through coating and occurrence of degradation process.

It should be mentioned that g-C_3N_4 materials are organic semi-conductors [47]. Further, we have functionalized the g-C_3N_4 materials with amine groups to enhance the compatibility between g-C_3N_4 materials and polymer matrice. Therefore, the g-C_3N_4 nanosheets act as insulating nanomaterial inside epoxy coating. The EIS results are fitted by the electrical equivalent circuits shown in Fig. 8; where R_s is the resistance of solution, R_{coat} is coating resistance, Q_{coat} is coating constant phase element, R_{ct} is charge transfer resistance, and Q_{dl} is the double layer constant phase element. Since the actual electrochemical processes are not a pure capacitor, constant phase elements are used instead of capacitors for modeling equivalent electrical circuits to obtain precise fitting results [48]. It should be mentioned that the EIS results are fitted by the help of Ivium software and the fitting quality of EIS data is evaluated by the Chi square (χ^2) test; in this regard, the value of χ^2 should decrease by tenfold if a new circuit element is introduced into the circuit model; indeed, if incorporation of a new circuit element does not substantially improve the goodness-of-fit via reducing the χ^2 value and relative errors, the

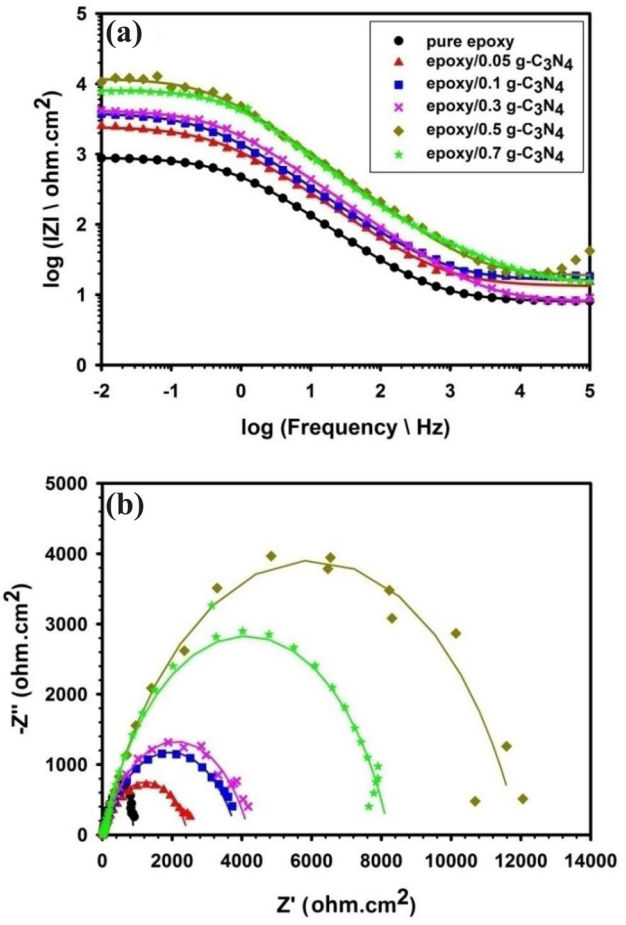

Fig. 5 **a** Bode and **b** Nyquist plots of epoxy coatings containing different wt% of AF g-C_3N_4 after 2 h immersion in 3.5 wt% NaCl solution

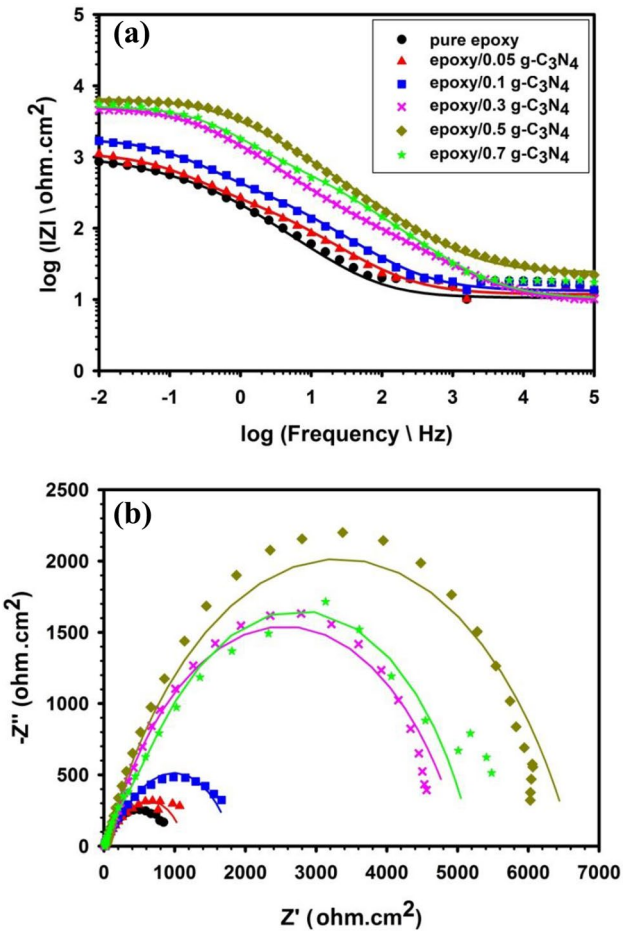

Fig. 6 **a** Bode and **b** Nyquist plots of epoxy coatings containing different wt% of AF g-C_3N_4 after 24 h immersion in 3.5 wt% NaCl solution

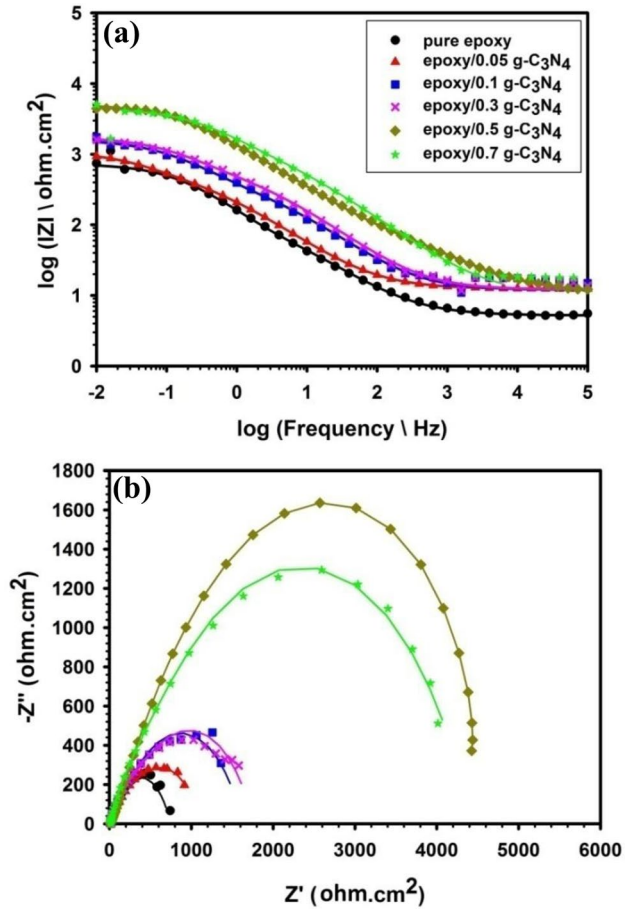

Fig. 7 **a** Bode and **b** Nyquist plots of epoxy coatings containing different wt% of AF g-C_3N_4 after 48 h immersion in 3.5 wt% NaCl Solution

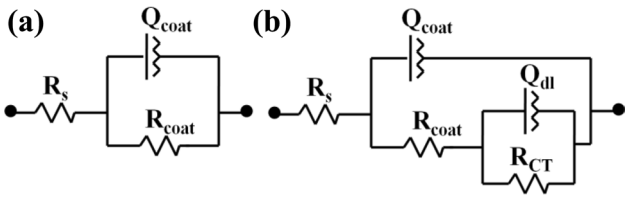

Fig. 8 Equivalent electrical circuits used for fitting EIS results after immersion for **a** 2 h and **b** 24 h and 48 h

simpler circuit is accepted and/or the search for an improved circuit is done [15].

Table 2 presents the fitted electrochemical parameters derived from EIS tests. R_{coat} and R_{ct} are two main parameters for evaluating the corrosion protection performance of coatings on metallic substrates. R_{coat} indicates the resistance of coating against diffusion of corrosive agents and R_{ct} presents the resistance of electron transfer across the metal [4]. Also, impedance modulus (|Z|) at low frequencies 10^{-2} Hz is presented in Table 2, which indicates the total resistance of coating system against corrosive media. The nanocomposite coatings exhibit higher values of R_{coat} and R_{ct}. The enhancement of R_{coat} and R_{ct} via addition of AF g-C_3N_4 reflects the better protective properties of coating systems. Further, the decrease of R_{coat} and R_{ct} with the immersion time indicates the degradation of coating as a result of water permeation in the coating. The results of EIS are compatible with FE-SEM images (Fig. 4), indicating that well-distributed g-C_3N_4 nanosheets in polymer matrix can provide higher corrosion resistance coatings. The increase of R_{ct} can be discussed from two aspects; the g-C_3N_4 nanosheets can provide more tortuous path ways for corrosive agents and further, these nanofiller decrease the coating porosity; therefore, the amount of corrosive agents at coating/metal interface decreases and R_{ct} increases. Further, the amine functionalized g-C_3N_4 nanosheets can increase the coating adhesion to metallic substrate and decrease the failure at coating/metal interface which is another parameter for enhancing the R_{ct} value. Indeed, nanocomposite coatings containing 0.5 wt% AF g-C_3N_4 nanosheets show the highest value of R_{coat} and R_{ct} which is because of well-distribution of nanosheets inside polymer matrice. However, by adding higher amounts of nanofiller (i.e. 0.7 wt%), the R_{ct} and R_{coat} values decrease which is attributed to agglomeration of nanosheets, developing pores within coatings and increasing the diffusion of corrosive agents within polymer matrice and failure at coating/metal interface.

The values of |Z| modulus, R_{coat}, and R_{ct} for nanocomposite coatings are significantly higher than pure epoxy coating at different immersion times. However, due to diffusion of corrosive agents through coating by increasing immersion time, the values of |Z| modulus, Rcoat, and Rct values decrease. It should be mentioned that the base epoxy coating used in this study shows limited corrosion protection; i.e. the resistance is in the range of 10^3 O cm^2. As a result, the improved resistance of prepared nanocomposite coatings is in the range of 10^4 O cm^2. Therefore, the corrosion protection performance of samples is investigated in the first hours of immersion. Similar behavior was observed in below studies [41, 49–51]. Moreover, the |Z| modulus, R_{coat}, and R_{ct} for pure epoxy coating is very low (i.e. $< 10^3$ O cm^2) and therefore, by increasing the immersion time, these parameters have not changed significantly. However, comparing the impedance parameters at every immersion time shows that the values of |Z| modulus, R_{coat}, and R_{ct} for nanocomposites are more than pure epoxy coating [52].

The value of coating capacitance (C_{coat}) is calculated based on Eq. 1 from constant phase element of protective coatings [53, 54]:

$$C_{coat} = \left(Y_0\right)^{1/n} \cdot \left(R_{coat}\right)^{(1-n)/n} \quad (1)$$

Table 2 The electrochemical parameters extracted from EIS data

Sample	Time	|Z| (Ω cm^2)	CPE_{coat}		R_{coat} (Ω cm^2)	CPE_{dl}		R_{CT} (Ω cm^2)
			Y_0 (Ω^{-1} cm^{-2} s^n)	n		Y_0 (Ω^{-1} cm^{-2} s^n)	n	
Pure epoxy	2 h	913.3	3.8×10^{-4}	0.71	892	–	–	–
	24 h	859.9	1.29×10^{-3}	0.74	408.4	4.86×10^{-3}	0.70	586.5
	48 h	744	1.09×10^{-3}	0.70	128	5.61×10^{-4}	0.74	608
Epoxy/0.05 AF g-C_3N_4	2 h	2530	1.91×10^{-4}	0.70	2452	–	–	–
	24 h	1107	1.35×10^{-3}	0.70	294.8	5.32×10^{-4}	0.71	847.4
	48 h	936.3	1.52×10^{-3}	0.70	237.6	3.15×10^{-3}	0.70	851.5
Epoxy/0.1 AF g-C_3N_4	2 h	3746	1.57×10^{-4}	0.70	3848	–	–	–
	24 h	1693	3.11×10^{-4}	0.71	447.2	6.82×10^{-4}	0.70	1364
	48 h	1736	3.36×10^{-4}	0.73	371.5	7.29×10^{-4}	0.70	1233
Epoxy/0.3 AF g-C_3N_4	2 h	4202	1.10×10^{-4}	0.71	4205	–	–	–
	24 h	4579.1	1.04×10^{-4}	0.67	216.1	6.10×10^{-5}	0.74	4845.3
	48 h	1606	2.81×10^{-4}	0.73	578.3	8.25×10^{-4}	0.70	1161
Epoxy/0.5 AF g-C_3N_4	2 h	10,650	4.44×10^{-5}	0.74	11,920	–	–	–
	24 h	7583.3	7.09×10^{-5}	0.65	102.3	7.40×10^{-5}	0.69	8608.9
	48 h	5060	1.14×10^{-4}	0.67	321.8	6.30×10^{-5}	0.75	5407.6
Epoxy/0.7 AF g-C_3N_4	2 h	7654.3	5.48×10^{-5}	0.70	8250	–	–	–
	24 h	5506	6.51×10^{-5}	0.72	1141	7.99×10^{-5}	0.79	4067
	48 h	5034.3	1.58×10^{-4}	0.70	417.2	1.62×10^{-4}	0.73	3981

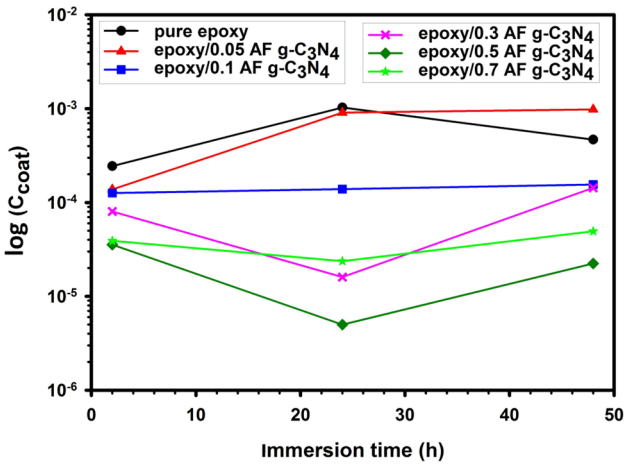

Fig. 9 The variation of C_{coat} for epoxy/AF g-C_3N_4 samples during immersion in NaCl solution

The variation of C_{coat} for samples during immersion is shown in Fig. 9 which indicates that the C_{coat} decreases via incorporating AF g-C_3N_4 in epoxy matrix. The lowest C_{coat} is observed for epoxy/0.5 AF g-C_3N_4 sample. Indeed, the presence of AF g-C_3N_4 nanosheets in coating can decrease the water uptake into the coating via decreasing the micro-pores and defects of polymer matrix. The fluctuation of C_{coat} during immersion can be considered from two different aspects; one trend is increasing of C_{coat} by increasing immersion time and water permeation in coating which is attributed to the higher dielectric constant of water compared to polymer matrix. The other trend is decreasing of C_{coat} during immersion which is due to filling the micro-pores of coating with corrosion products [46]. Accordingly, the compatibility between AF g-C_3N_4 nanosheets and epoxy matrix has lead to higher degrees of cross-linking in the coating. Also, the micro-pores of coating have decreased by adding AF g-C_3N_4 in the coating, providing higher levels of compactness and improved barrier performance. However, the C_{coat} increases when extra amounts of nanofiller (0.7 wt%) is added in the coating and the protection efficiency of coating decreases, which can be assigned to agglomeration and packing re-union of AF g-C_3N_4 nanosheets in the polymer coating and producing defects in the matrix according to FE-SEM images presented in Fig. 4. The corrosive electrolyte can diffuse through these defects and deteriorate the protection efficiency of coating [55].

The behavior of coating is discussed based on the calculated results for C_{coat} according to Eq. 1 accompanied by FE-SEM images presented in Fig. 4. The results clearly show that the value of C_{coat} decreases by adding g-C_3N_4 nanosheets within epoxy coatings, indicating decreasing the water absorption by nanocomposite coatings. The decrease of C_{coat} in the case of nanocomposite coatings can be attributed to decrease of coating porosity and increase of interfacial interactions between polymer and nanofiller. Meanwhile epoxy coatings loaded with 0.5 wt% g-C_3N_4 nanosheets show the lowest values of C_{coat} during

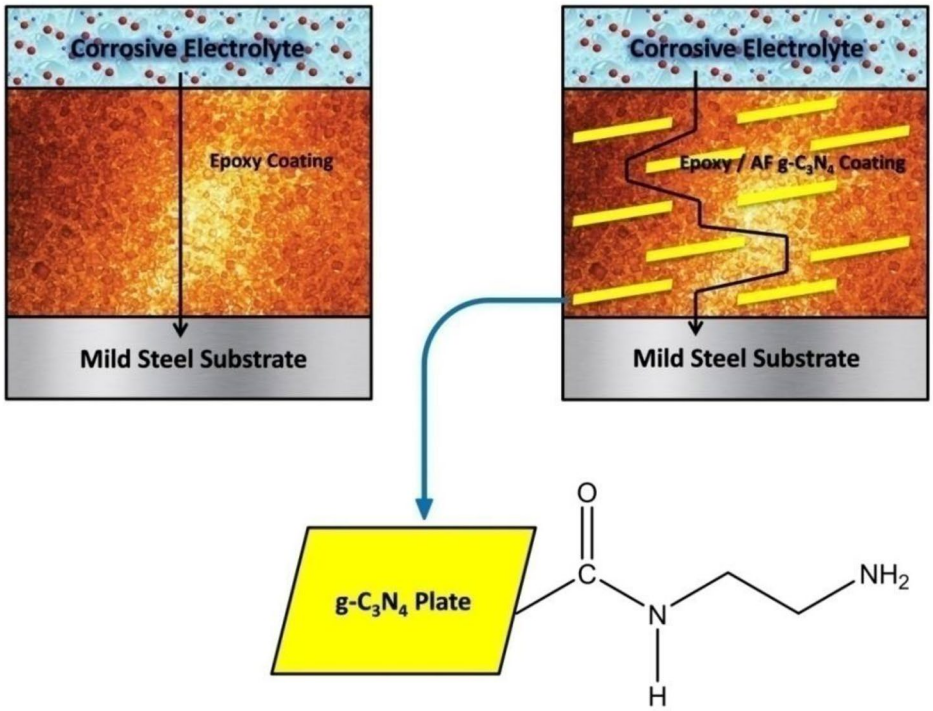

Fig. 10 Schematic of corrosion protection mechanism for pure epoxy and epoxy/AF g-C_3N_4 nanocomposite coatings

immersion, which can be assigned to uniform dispersion of g-C_3N_4 within polymer matrice and decreasing the defects of coating [53–55].

3.4 Corrosion protection mechanism of epoxy/AF g-C_3N_4 nanocomposite coatings

As EIS results show, pure epoxy coatings show significantly low corrosion protection due to formation of defects and pores in the polymer coating during its application and curing process on mild steel substrate. Corrosive electrolyte easily diffuses in pure epoxy coating through the pores and cavities. The permeation of corrosive electrolyte can lead to hydrolytically destruction of epoxy coating and the hydrogen bonds between epoxy coating and the metal surface deteriorates [5, 9]. Therefore, the corrosive agents including H_2O and O_2 accumulate at coating/metal interface and the following corrosion reactions occur [8]:

$$\text{Anodic reaction}: \ Fe \rightarrow Fe^{2+} + 2e^{-} \quad (2)$$

$$\text{Cathodic reaction}: \ H_2O + {}^1/_2\, O_2 + 2e^{-} \rightarrow 2OH^{-} \quad (3)$$

Therefore, in this research, g-C_3N_4 sheets are incorporated in epoxy coating in order to reduce the diffusion of corrosive agents into metal/coating interface. The g-C_3N_4 sheets are chemically modified with the vapors of ethylenediamine via a simple method. In the developed method, the AF g-C_3N_4 sheets can easily be dispersed in polyamide hardener without using long-lasting ultrasonic methods. The amine groups (NH_2) improve the compatibility and interfacial bonding between g-C_3N_4 sheets and the polyamide hardener and enhance the dispersion quality of g-C_3N_4 sheets in epoxy coating. The well-dispersed AF g-C_3N_4 sheets in polymer matrix can increase the tortuosity of diffusion path for corrosive agents such as H_2O and O_2 [3]. From the other point of view, the cross-link density of epoxy coating enhances by adding AF g-C_3N_4 due to the presence of amine groups on g-C_3N_4 sheets and also, strong chemical bond creates between composite coating and metal surface. Therefore, the deterioration rate of composite coatings decreases. Figure 10 schematically shows the corrosion protection mechanism of epoxy/AF g-C_3N_4 nanocomposite coatings.

Meanwhile, the amount of AF g-C_3N_4 in epoxy coating is an important parameter for achieving higher corrosion resistance. The corrosion resistance of epoxy coatings enhances by increasing the amount of AF g-C_3N_4 in polymer matrix. As AF g-C_3N_4 is added above the optimum value (which is 0.5 wt% in this study), the AF g-C_3N_4 nanosheets agglomerate in coating and the number of defects and cracks grows which facilitates the diffusion of corrosive medium [30].

4 Conclusion

We have successfully synthesized g-C_3N_4 from melamine via a simple two-step condensation process including hydrothermal treatment of melamine and then its

polymerization in the presence of ammonium carbonate. The prepared g-C_3N_4 is further characterized with XRD and TEM. The corrosion inhibition performance of g-C_3N_4 as nanofiller in solvent based epoxy coatings is investigated. In order to enhance the dispersion quality of g-C_3N_4 in polymer matrix, it is functionalized with amine vapor which is a facile method without separation and drying steps. The functionalization of g-C_3N_4 is confirmed by FT-IR analysis. The corrosion resistance of epoxy coatings loaded with 0, 0.05, 0.1, 0.3, 0.5, and 0.7 wt% amine functionalized g-C_3N_4 is evaluated by EIS. In the initial of EIS studies, epoxy coating containing 0.5 wt% AF g-C_3N_4 shows the highest impedance modulus of 10,650 Ω.cm^2 compared to pure epoxy sample (913 Ω cm^2). By increasing the immersion time to 48 h, the impedance modulus of epoxy/0.5 AF g-C_3N_4 and pure epoxy coating decreases to 5060 and 744 Ω cm^2, respectively; due to diffusion of aggressive agents into coating/metal interface. Accordingly, it turned out that AF g-C_3N_4 can significantly improve the barrier performance of epoxy coatings.

Funding This study was funded by Iranian Elite National Foundation (Bonyad Melli Nokhbegan) as Allameh Tabatabaei's Award for financial support.

Compliance with ethical standards

Conflict of interest The authors declare that they have no conflict of interest.

References

1. Curtzwiler GW, Williams EB, Maples AL, Wand SW, Rawlins JW (2017) Measurable and influential parameters that influence corrosion performance differences between multiwall carbon nanotube coating material combinations and model parent material combinations derived from epoxy-amine matrix materials. ACS Appl Mater Interfaces 9(7):6356–6368
2. He P, Wang J, Lu F, Ma Q, Wang Z (2017) Synergistic effect of polyaniline grafted basalt plates for enhanced corrosion protective performance of epoxy coatings. Prog Org Coat 110:1–9
3. Zuo S, Chen Y, Liu W, Yao C, Li Y, Ma J, Kong Y, Mao H, Li Z, Fu Y (2017) Polyaniline/g-C_3N_4 composites as novel media for anticorrosion coatings. J Coat Technol Res. https://doi.org/10.1007/s11998-017-9916-7
4. Zheng H, Shao Y, Wang Y, Meng G, Liu B (2017) Reinforcing the corrosion protection property of epoxy coating by using graphene oxide–poly(urea–formaldehyde) composites. Corros Sci 123:267–277
5. Ganjaee Sari M, Shamshiri MR, Ramezanzadeh B (2017) Fabricating an epoxy composite coating with enhanced corrosion resistance through impregnation of functionalized graphene oxide-co-montmorillonite nanoplatelet. Corros Sci 129:38–53
6. Kongparakul S, Kornprasert S, Suriya P, Le D, Samart C, Chantarasiri N, Prasassarakich P, Guan G (2017) Self-healing hybrid nanocomposite anticorrosive coating fromepoxy/modified nanosilica/perfluorooctyl triethoxysilane. Prog Org Coat 104:173–179
7. Pourhashem S, Rashidi AM, Vaezi MR, Bagherzadeh MR (2017) Excellent corrosion protection performance of epoxy composite coatings filled with amino-silane functionalized graphene oxide. Surf Coat Technol 317:1–9
8. Chang CH, Huang TC, Peng CW, Yeh TC, Lu H, Hung W, Weng CJ, Yang T, Yeh JM (2012) Novel anticorrosion coatings prepared from polyaniline/graphene composites. Carbon 50:5044–5051
9. Chang KC, Hsu MH, Lu H, Lai MC, Liu PJ, Hsu CH, Ji WF, Chuang TL, Wei Y, Yeh JM, Liu WR (2014) Room-temperature cured hydrophobic epoxy/graphene composites as corrosion inhibitor for cold-rolled steel. Carbon 66:144–153
10. Yi M, Shen Z, Zhao X, Liu L, Liang S, Zhang X (2014) Exploring few-layer graphene and graphene oxide as fillers to enhance the oxygen-atom corrosion resistance of composites. Phys Chem Chem Phys 16:11162–11167
11. Haeri SZ, Asghari M, Ramezanzadeh B (2017) Enhancement of the mechanical properties of an epoxy composite through inclusion of graphene oxide nanosheets functionalized with silica nanoparticles through one and two steps sol–gel routes. Prog Org Coat 111:1–12
12. Liu S, Gu L, Zhao H, Cheng J, Yu H (2016) Corrosion resistance of graphene reinforced waterborne epoxy coatings. J Mater Sci Technol 32(5):425–431
13. Karimi B, Ramezanzadeh B (2017) A comparative study on the effects of ultrathin Luminescent graphene oxide quantum dot (GOQD) and graphene oxide (GO) nanosheets on the interfacial interactions and mechanical properties of an epoxy composite. J Colloid Interface Sci 493:62–76
14. Sun W, Wang L, Wu T, Wang M, Yang Z, Pan Y, Liu G (2015) Inhibiting the corrosion-promotion activity of graphene. Chem Mater 27:2367–2373
15. Pourhashem S, Vaezi MR, Rashidi AM, Bagherzadeh MR (2017) Exploring corrosion protection properties of solvent based epoxy-graphene oxide nanocomposite coatings on mild steel. Corros Sci 115:78–92
16. Krishnamoorthy K, Jeyasubramanian K, Premanathan M, Subbiah G, Shin HS, Kim SJ (2014) Graphene oxide nanopaint. Carbon 72:328–337
17. Huang HD, Ren PG, Chen J, Zhang WQ, Ji X, Li ZM (2012) High barrier graphene oxide nanosheet/poly(vinyl alcohol) nanocomposite films. J Membr Sci 409–410:156–163
18. Pourhashem S, Vaezi MR, Rashidi AM, Bagherzadeh MR (2017) Distinctive roles of silane coupling agents on the corrosion inhibition performance of graphene oxide in epoxy coatings. Prog Org Coat 111:47–56
19. Ramezanzadeh B, Niroumandrad S, Ahmadi A, Mahdaviana M, Mohamadzadeh Moghadam MH (2016) Enhancement of barrier and corrosion protection performance of an epoxy coating through wet transfer of amino functionalized graphene oxide. Corros Sci 103:283–304
20. Pourhashem S, Vaezi MR, Rashidi AM (2017) Investigating the effect of SiO_2-graphene oxide hybrid as inorganic nanofiller on corrosion protection properties of epoxy coatings. Surf Coat Technol 311:282–294
21. Yu Z, Di H, Ma Y, He Y, Liang L, Lv L, Ran X, Pan Y, Luo Z (2015) Preparation of graphene oxide modified by titanium dioxide to enhance the anti-corrosion performance of epoxy coatings. Surf Coat Technol 276:471–478
22. Yu Z, Di H, Ma Y, Lv L, Pan Y, Zhang C, He Y (2015) Fabrication of graphene oxide–alumina hybrids to reinforce the anti-corrosion performance of composite epoxy coatings. Appl Surf Sci 351:986–996
23. Lakhi KS, Park DH, Al-Bahily K, Cha W, Viswanathan B, Choy JH, Vinu A (2017) Mesoporous carbon nitrides: synthesis, functionalization, and applications. Chem Soc Rev 46:72–101

24. Bellardita M, García-López EI, Marcì G, Krivtsov I, Garcí JR, Palmisano L (2018) Selective photocatalytic oxidation of aromatic alcohols in water by using P doped g-C_3N_4. Appl Catal B Environ 220:222–233
25. Gao J, Wang Y, Zhou S, Lin W, Kong Y (2017) A facile one-step synthesis of Fe-doped g-C_3N_4 nanosheets and their improved visible-light photocatalytic performance. ChemCatChem 9:1708–1715
26. Fang HB, Luo Y, Zheng YZ, Ma W, Tao X (2016) Facile large-scale synthesis of urea-derived porous graphitic carbon nitride with extraordinary visible-light spectrum photodegradation. Ind Eng Chem Res 55(16):4506–4514
27. Shi Y, Jiang S, Zhou K, Bao C, Yu B, Qian X, Wang B, Hong N, Wen P, Gui Z, Hu Y, Yuen RKK (2014) Influence of g-C_3N_4 nanosheets on thermal stability and mechanical properties of biopolymer electrolyte nanocomposite films: a novel investigation. ACS Appl Mater Interfaces 6:429–437
28. Yan H, Chen Y, Xu S (2012) Synthesis of graphitic carbon nitride by directly heating sulfuric acid treated melamine for enhanced photocatalytic H_2 production from water under visible light. Int J Hydrog Energy 37:125–133
29. Shi Y, Wang B, Duan L, Zhu Y, Gui Z, Yuen RKK, Hu Y (2016) Processable dispersions of graphitic carbon nitride based nanohybrids and application in polymer nanocomposites. Ind Eng Chem Res 55(28):7646–7654
30. Mo M, Zhao W, Chen Z, Yu Q, Zeng Z, Wu X, Xue Q (2015) Excellent tribological and anti-corrosion performance of polyurethane composite coatings reinforced with functionalized graphene and graphene oxide nanosheets. RSC Adv 5:56486–56497
31. Wang R, Zhuo D, Weng Z, Wu L, Cheng X, Zhou Y, Wang J, Xuan B (2015) A novel nanosilica/graphene oxide hybrid and its flame retarding epoxy resin with simultaneously improved mechanical, thermal conductivity, and dielectric properties. J Mater Chem A 3:9826–9836
32. Supova M, Martynkova GS, Barabaszova K (2011) Effect of nanofillers dispersion in polymer matrices: a review. Sci Adv Mater 3(1):1–25
33. Wei J, Atif R, Vo T, Inam F (2015) Graphene nanoplatelets in epoxy systems: dispersion, reaggregation, and mechanical properties of nanocomposites. J Nanomater. https://doi.org/10.1155/2015/561742
34. Xia W, Jin C, Kundu S, Muhler M (2009) A highly efficient gas-phase route for the oxygen functionalization of carbon nanotubes based on nitric acid vapor. Carbon 47:919–922
35. Unal S, Hunt RN, Hocke H (2012) Vapor phase functionalization of carbon nanotubes. US Patent (2012)/0234204 A1
36. Dong G, Zhang L (2012) Porous structure dependent photoreactivity of graphitic carbon nitride under visible light. J Mater Chem 22:1160–1166
37. Zhang S, Hang NT, Zhang Z, Yue H, Yang W (2017) Preparation of g-C_3N_4/graphene composite for detecting NO_2 at room temperature. Nanomaterials 7(1):1–12
38. Han K, Wang C, Li Y, Wan M, Wang Y, Zhu JH (2013) Facile template-free synthesis of porous g-C_3N_4 with high photocatalytic performance under visible light. RSC Adv 3:9465–9469
39. Feng D, Cheng Y, He J, Zheng L, Shao D, Wang W, Wang W, Lu F, Dong H, Liu H, Zheng R, Liu H (2017) Enhanced photocatalytic activities of g-C_3N_4 with large specific surface area via a facile one-step synthesis process. Carbon 125:454–463
40. Naderi M, Hoseinabadi M, Najafi M, Motahari S, Shokri M (2018) Investigation of the mechanical, thermal, and anticorrosion properties of epoxy nanocomposite coatings: Effect of synthetic hardener and nanoporous graphene. J Appl Polym Sci 135:46201(1)–46201(11)
41. Parhizkar N, Shahrabi T, Ramezanzadeh B (2017) A new approach for enhancement of corrosion protection properties and interfacial adhesion bonds between the epoxy coating and steel substrate through surface treatment by covalently modified amino functionalized graphene oxide. Corros Sci 123:55–75
42. Galpaya D, Wang M, George G, Motta N, Waclawik E, Yan C (2014) Preparation of graphene oxide/epoxy nanocomposites with significantly improved mechanical properties. J Appl Phys 116:0532518-(1)–0532518-(10)
43. Ma Y, Di H, Yu Z, Liang L, Lv L, Pan Y, Zhang Y, Yin D (2016) Fabrication of silica-decorated graphene oxide nanohybrids and the properties of composite epoxy coatings research. Appl Surf Sci 360:936–945
44. Zhu K, Li X, Wang H, Li J, Fei G (2016) Electrochemical and anticorrosion behaviors of water dispersible graphene/acrylic modified alkyd resin latex composites coated carbon steel. J Appl Polym Sci 134:44445 (1)–44445 (12)
45. Ramezanzadeh B, Haeri H, Ramezanzadeh M (2016) A facile route of making silica nanoparticles-covered graphene oxide nanohybrids (SiO_2-GO); fabrication of SiO_2-GO/epoxy composite coating with superior barrier and corrosion protection performance. Chem Eng J 303:511–528
46. Ghasemi-Kahrizsangi A, Shariatpanahi H, Nesgati J, Akbarinezah E (2015) Corrosion behavior of modified nano carbon black/epoxy coating in accelerated conditions. Appl Surf Sci 331:115–126
47. Silva AM, Rojas MI (2016) Electric and structural properties of polymeric graphitic carbon nitride (g-C_3N_4): a density and functional theory. Comput Theor Chem 1098:41–49
48. Yang P, Zhao J, Qiao W, Li L, Zhu Z (2015) Ammonia-induced robust photocatalytic hydrogen evolution of graphitic carbon nitrides. Nanoscale 7:18887–18890
49. Nikpour B, Ramezanzadeh B, Bahlakeh G, Mahdavian M (2017) Synthesis of graphene oxide nanosheets functionalized by green corrosion inhibitive compounds to fabricate a protective system. Corros Sci 127:240–259
50. Wu Y, Song N, Wang W, Zhao Y (2018) Synthesis of graphene/epoxy resin composite via 1,8- diaminooctane by ultrasonication approach for corrosion protection. Ultrason Sonochem 42:464–470
51. Contri G, Barra GMO, Ramoa SDAS, Merlini C, Ecco LG, Souza FS, Spinelli A (2018) Epoxy coating based on montmorillonite-polypyrrole: electrical properties and prospective application on corrosion protection of steel. Prog Org Coat 114:201–207
52. Zhan Y, Zhang J, Wan X, Long Z, He S, He Y (2018) Epoxy composites coating with Fe_3O_4 decorated graphene oxide: modified bio-inspired surface chemistry, synergistic effect and improved anti-corrosion performance. Appl Surf Sci 436:756–767
53. Hsu CH, Mansfeld F (2001) Concerning the conversion of the constant phase element parameter Y0 into a capacitance. Corrosion 57(9):747–748
54. Dang DN, Peraudeau B, Cohendoz S, Mallarino S, Feaugas X, Touzain S (2014) Effect of mechanical stresses on epoxy coating ageing approached by electrochemical impedance spectroscopy measurements. Electrochim Acta 124:80–89
55. Wang N, Zhang Y, Chen J, Zhang J, Fang Q (2017) Dopamine modified metal-organic frameworks on anti-corrosion properties of waterborne epoxy coatings. Prog Org Coat 109:126–134